

Propene concentration sensing for combustion gases using quantum-cascade laser absorption near 11 μm

Robin S. M. Chrystie¹ · Ehson F. Nasir¹ · Aamir Farooq¹

Received: 7 February 2015 / Accepted: 11 May 2015
© Springer-Verlag Berlin Heidelberg 2015

Abstract We report on a strategy to measure, in situ, the concentration of propene (C_3H_6) in combustion gases using laser absorption spectroscopy. Pyrolysis of *n*-butane was conducted in a shock tube, in which the resultant gases were probed using an extended cavity quantum-cascade laser. A differential absorption approach using online and offline wavelengths near $\lambda = 10.9 \mu\text{m}$ enabled discrimination of propene, cancelling the effects of spectral interference from the simultaneous presence of intermediate hydrocarbon species during combustion. Such interference-free measurements were facilitated by exploiting the =C–H bending mode characteristic to alkenes (olefins). It was confirmed, for intermediate species present during pyrolysis of *n*-butane, that their absorption cross sections were the same magnitude for both online and offline wavelengths. Hence, this allowed time profiles of propene concentration to be measured during pyrolysis of *n*-butane in a shock tube. Time profiles of propene subsequent to a passing shock wave exhibit trends similar to that predicted by the well-established JetSurF 1.0 chemical kinetic mechanism, albeit lower by a factor of two. Such a laser diagnostic is a first step to experimentally determining propene in real time with sufficient time resolution, thus aiding the refinement and development of chemical kinetic models for combustion.

1 Introduction

Laser diagnostics used in combustion applications are invaluable in addressing issues related to process efficiency, performance, and pollution. Laser diagnostics assist in the development of computational tools, which ultimately empower engineers to effectively design and develop improved combustion technology. Chemical kinetic models form a pivotal component of these computational tools. Detailed models of realistic fuels comprise thousands of species and tens of thousands of chemical reactions. Development of these models requires robust testing against experimental data. Laser-based diagnostics are now typically acknowledged to be capable of providing such robust testing, thus facilitating the development of reliably accurate kinetic models to ultimately improve the computational design capability towards improved combustion technology.

New combustion concepts, such as lean premixed prevapourized (LPP) gas turbines and reactivity-controlled compression ignition (RCCI) engines, tend to be based on lean, low-temperature, and high-pressure conditions, chiefly in order to reduce soot and NO_x emissions. In the case of LPP technology, temperature was determined to be one of the main determinants of process behaviour [1, 2]. However, under such homogeneously lean conditions the rate of reaction tends to be rate limiting and it is, therefore, very important to study the role of chemical kinetics in understanding and controlling such process behaviour. This would involve the development, testing, and improvement of chemical kinetic models for a particular fuel used. One of the traditional methods of testing such models is to compare the predicted ignition delay time with that from shock tube experiments. However, more accurate and comprehensive model testing has been increasingly taking a

✉ Aamir Farooq
aamir.farooq@kaust.edu.sa

¹ Clean Combustion Research Centre, Division of Physical Sciences and Engineering, King Abdullah University of Science and Technology (KAUST), Thuwal 23955-6900, Saudi Arabia

multivariable approach through the measurement of species concentrations and temperature time profiles [3–7], chiefly using laser diagnostics.

Detailed investigation of hydrocarbon intermediates, for example, is important for understanding reaction paths controlling overall fuel consumption [8] and pollutant formation [9]. In particular, the overall rate of fuel consumption can be a strong function of alkene chemistry [10]. It is, therefore, paramount to gain refined knowledge of the formation and decay rates of various alkenes [11–17].

Propene (C_3H_6) is a relatively abundant alkene intermediate present in combustion gases. Propene is gathering interest in the kinetics community because of its important role in combustion chemistry [12–17]. The abundance of propene as a by-product of combustion is due to its molecular stability and serves as a reliable marker of combustion inefficiency in internal combustion engines [18]. Propene emission into the atmosphere poses the greatest threat with respect to ground-level photochemical ozone formation [9], and therefore it is of interest to minimize its emission. Soot abatement is also a high priority, with particulate matter originating from the propargyl radical $\bullet C_3H_3$. Propene leads a direct pathway to the creation of propargyl, which readily forms the benzene molecule during combustion [19]. Benzene, similar to other aromatics, leads to the formation of polycyclic aromatic hydrocarbons and subsequent particulate matter.

The concentration and residence time profile of propene formed during combustion, and its consequences downstream, can be controlled by the chemical profile of the fuel burned and influenced by molecular size, molecular branching, degree of saturation and aromaticity, and degree of oxygenation or nitration [20]. Fuel formulation may be guided by better insight via quantitative measurements of propene formed during combustion, using laser diagnostics, in order to ultimately (1) minimize residual soot from engine exhaust, (2) reduce ground-level ozone formation in cities, and (3) control knock in engines.

Direct measurement of propene has traditionally involved physical sampling using probes [21]. This approach is very effective at detecting many species within a single measurement. Unfortunately, it is an invasive procedure and is generally less straightforward to implement compared to laser diagnostic approaches. Most importantly, physical sampling does not offer a sufficient degree of time resolution compared to laser diagnostics, and therefore is not ideally suited to rapidly evolving chemical reactions taking place inside a shock tube. A more recent approach to overcome the limitations of physical sampling is to use an electronic sensor. Samman et al. [22] used a MOSiC (SiC-based metal-oxide semiconductor) sensor which showed signs of species specificity, including that towards propene. However, there is still relatively slow time response of such

sensors (~ 100 ms). More recently, there have been developments in optical absorption sensing of small hydrocarbon intermediates in shock tube environments, namely CH_4 [23, 24], C_2H_4 [25], C_2H_2 [26], and $i-C_4H_8$ [11]. Hitherto, to the best of our knowledge, there is no reported laser absorption diagnostic for the C-3 hydrocarbon propene (C_3H_6). The optical approach offers many advantages such as the ability to readily perform in situ measurements with excellent time resolution without perturbing the system environment.

The specific objective of the current work is to develop a highly time-resolved, non-invasive, and accurate in situ laser diagnostic based on absorption spectroscopy for measuring the composition of propene (C_3H_6) in a shock tube environment. Such a diagnostic would facilitate the ultimate goal of chemical kinetic model development and validation.

2 Diagnostic scheme

2.1 Likely intermediates

In order to effectively devise a sensing strategy for the propene (C_3H_6) intermediate during combustion, a preliminary check of the likely major molecular species formed during pyrolysis and oxidation of *n*-butane (a simple and well-studied fuel) was performed using the JetSurF 1.0 kinetic mechanism [27]. Such identification of intermediate species highlights molecules that could potentially lead to spectroscopic interference and hence guides the sensing strategy to be invoked. Figure 1a shows dominant species formed during the pyrolysis of 5 % *n*-butane at representative combustion conditions (1350 K, 3.5 bar). The dominant species are primarily stable hydrocarbon molecules. At the conditions of Fig. 1a, appreciable quantities of propene are formed (~ 1 %), equating to about 20 % of the initial loading of *n*-butane here.

At similar conditions, stoichiometric oxidation of 1 % *n*-butane yields the predicted species time profile shown in Fig. 1b. One per cent loading was chosen as 5 % would otherwise result in large energy release in shock tube experiments. Large energy release leads to departure from ideal shock tube behaviour, and thus a smaller and more appropriate initial loading was chosen. The simulation predicts about 0.2 % peak formation of propene along with several other hydrocarbons, radicals, and product species. In general, oxidation of fuels results in hydrocarbon intermediate species being formed and consumed in a relatively short period of time, as exemplified by the first ~ 500 μs shown in Fig. 1b. In this study, we have focused on developing a propene diagnostic for fuel pyrolysis to provide an early demonstration of propene sensing.

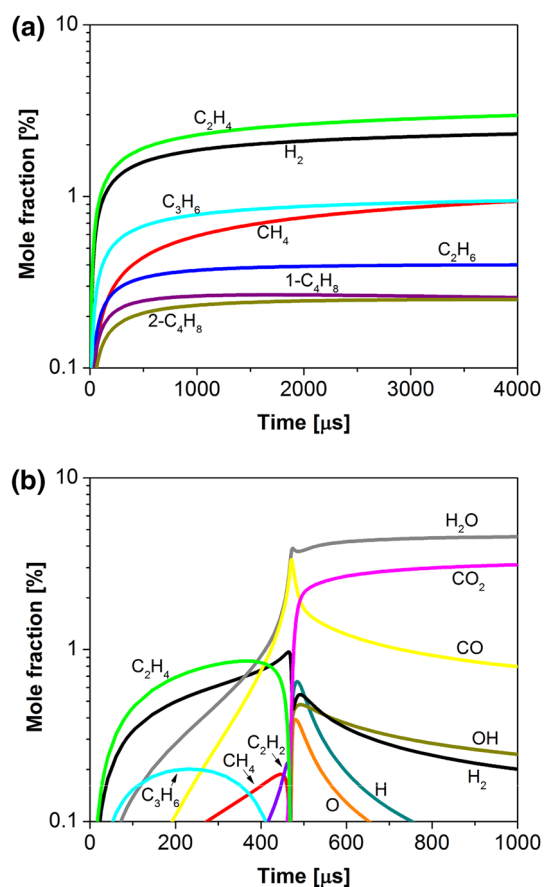


Fig. 1 Simulated history of major species generated during **a** pyrolysis of 5 % *n*-butane in argon and **b** oxidation of stoichiometric 1 % *n*-butane/ O_2 /Ar mixture. Initial temperature and pressure for both cases are 1350 K and 3.5 bar. Simulations are performed using CHEMKIN-PRO [28] with the JetSurF 1.0 chemical kinetic mechanism [27]

2.2 Selection of probe wavelength

Given a preliminary audit of the major (>0.1 %) likely intermediate species for 5 % *n*-butane pyrolysis has been conducted, a subset of spectroscopically relevant molecules can be identified. In regard to the application of spectroscopy, all molecules identified in Fig. 1a, except H_2 , are responsive to infrared radiation. The infrared region is ideal due to high spectral resolution, well-characterized transitions, and wide availability of radiation sources. In particular, the mid infrared (MIR) spectral region offers the strongest transitions due to the existence of the dominant fundamental vibrational bands and, furthermore, results in less interference from fewer species; these two aspects are favourable when devising a sensing strategy. Less interference implies that the spectral contribution originating from the target species (propene in this study) can be more easily discriminated from the aggregate signal. Less spectral interference consequently requires fewer measurements to yield

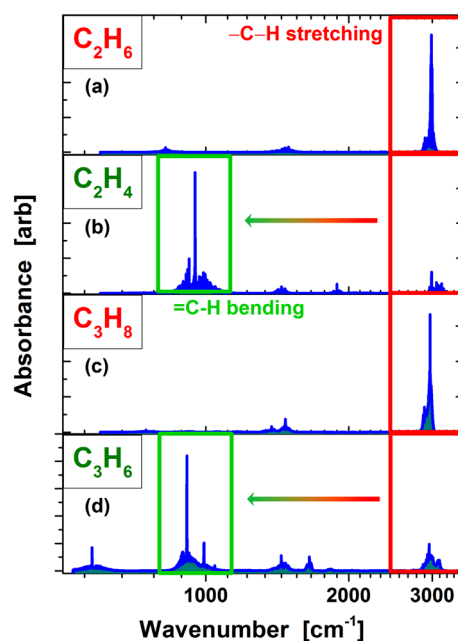


Fig. 2 Infrared absorption spectra of C-2 and C-3 alkanes (**a**, **c**) and alkenes (**b**, **d**). Region of the $-C-H$ stretching mode near 3000 cm^{-1} (conventionally used) is compared to the region of the $=C-H$ bending mode near 1000 cm^{-1} (used in this work)

a unique solution and therefore also results in improved accuracy of inferred species concentration derived from the aggregate spectra.

Figure 2 shows example infrared spectra for C-2 and C-3 hydrocarbons relevant to *n*-butane pyrolysis. It is evident that both alkanes and alkenes possess vibrational bands located around 3000 cm^{-1} , outlined in red in Fig. 2. Such bands are due to the $-C-H$ stretching mode of hydrocarbon molecules.

However, there also exist bands further into the MIR region that are characteristic to alkenes, outlined in green in Fig. 2. Such bands which lie around 1000 cm^{-1} are attributable to the $=C-H$ bending mode of the alkene molecules. Detection at this spectral location clearly enables discrimination against potential spectral interference from alkanes present in the combustion mixture, since alkanes do not absorb near 1000 cm^{-1} . It was therefore decided to devise a sensing strategy using wavelengths near $10\text{ }\mu\text{m}$ (1000 cm^{-1}), allowing for the elimination of all alkanes (CH_4 , C_2H_6 , C_3H_8 etc.) as considerable spectral interferents. Fortuitously, this scheme can be realized with today's advances in MIR technology, which have realized the availability of sufficiently sensitive detectors and quantum-cascade lasers (QCLs) near $10\text{ }\mu\text{m}$.

After elimination of the possibility of many spectroscopically interfering species, it is more feasible to use a differential absorbance scheme to overcome interference from the remaining species. The differential absorbance scheme

can be summarized by Eqs. (1–4). Absorption of monochromatic radiation is described by the Beer–Lambert law:

$$\ln(I_o/I) = \alpha(\lambda, T, P, X, L) = \sigma(\lambda, T, P) \cdot PXL/RT \quad (1)$$

where I/I_o is the fractional transmission, $\sigma(\lambda, T, P)$ is the absorption cross section, and $\alpha(\lambda, T, P, X, L)$ is the spectral absorbance, with associated dependencies on wavelength (λ), temperature (T), pressure (P), composition (X), and path length (L). Equation (1) can be modified to accommodate additional absorption contributions from molecular interferents and extinction (ε) from scattering sources. These two terms are represented in parentheses within Eq. (2), which contribute further to the absorbance originating from the target species (propene).

$$\ln(I_o/I) = \alpha_{\text{propene}} + (\alpha_{\text{interferents}} + \varepsilon) \quad (2)$$

The differential absorbance scheme relies on the combined spectral quantity, $(\alpha_{\text{interferents}} + \varepsilon)$, to be independent of wavelength within a reasonable spectral range. This enables the possibility of invoking the two-colour technique to obviate the need for measuring compositions of all interfering species, in order to infer the propene concentration. Equation (3) represents the differential absorbance scheme, involving separate measurements at two slightly different spectral locations, indicated by the terms *online* and *offline*.

$$\ln(I_o/I)_{\text{online}} - \ln(I_o/I)_{\text{offline}} \cong (\alpha_{\text{propene}})_{\text{online}} - (\alpha_{\text{propene}})_{\text{offline}} \quad (3)$$

Equation (3) assumes its simple form, as a consequence of the invariance of $(\alpha_{\text{interferents}} + \varepsilon)$ between online and offline measurements, and hence its cancellation in the differential absorbance scheme. Combination of Eqs. (1) and (3) results in Eq. (4), in which the differential absorption cross section is given by:

$$\Delta\sigma = \sigma_{\text{propene}}(\text{online}) - \sigma_{\text{propene}}(\text{offline}).$$

$$X_{\text{propene}} = \frac{\ln\left(\left(\frac{I_o}{I}\right)_{\text{online}} / \left(\frac{I_o}{I}\right)_{\text{offline}}\right)}{\Delta\sigma \cdot PL/RT} \quad (4)$$

This, in principle, allows propene concentration to be inferred in the presence of interferents and scattering using the method of differential absorbance outlined above. Naturally, such a scheme works effectively when the background interfering absorption spectra are featureless, this being typical of large hydrocarbons. Figure 3a shows overlapping absorption cross-sectional spectra [29] of the =C–H bending mode band near 1000 cm^{-1} for four spectrally relevant alkenes during *n*-butane pyrolysis.

In this case, the larger alkene molecules, such as the two butenes and to some extent propene, are generally lacking much spectral fine structure over the 100 cm^{-1} range shown in Fig. 3a. Figure 3b, which highlights the region of interest of Fig. 3a, manifests the correlation between

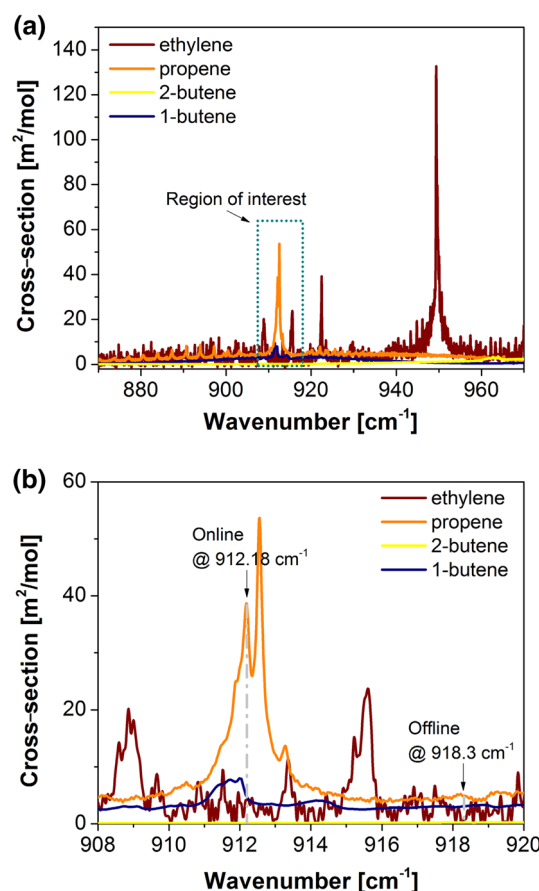


Fig. 3 a Absorption cross-sectional profiles of propene and accompanying interferents at 298 K, 1 atm; spectral resolution of $\sim 0.1 \text{ cm}^{-1}$. b Detailed view of absorption cross section for propene and interferents at the region of interest in a, showing the selected online (912.18 cm^{-1}) and offline (918.3 cm^{-1}) wavelengths used in this study

spectral structure and molecular size. For a C-2 molecule, such as ethylene, there is far more fine structure compared to other interferent molecules (e.g. 1-butene and 2-butene). For propene measurements in this work, the offline location of 918.3 cm^{-1} was chosen because the ethylene cross section there is on parity with that of the online location at 912.18 cm^{-1} , despite the structure of the ethylene spectrum. Therefore, with careful selection of the wavelength, the differential absorbance technique can be exploited for interference-free measurements when the interferents themselves possess structured spectra. Such data to support this assertion are presented in Sect. 4.1 of the paper.

To summarize the principles involved in selecting the most appropriate wavelengths for the differential absorbance scheme used in this study, the following guidelines are listed.

Selection guideline 1:

An initial aim to dramatically reduce the number of potential interferent molecules, by identifying a spectral attribute

that is unique to the class of target molecule or to the target molecule itself. In this study, the =C–H bending mode is characteristic to alkenes (olefins), thus allowing to filter out the spectral effects of the presence of alkanes

Selection guideline 2:

Once a general spectral region has been narrowed down, by invoking guideline 1, the availability of laser sources must be assessed. In the case of alkene-specific spectral fingerprints in this study, the region around 1000 cm^{-1} ($10\text{ }\mu\text{m}$) can be easily accessed using CO_2 gas lasers or QCLs

Selection guideline 3:

At the temperatures of interest within the study, the absorption cross section at the online spectral location should be maximized towards optimum SNR. For propene sensing here, the peak at 912.18 cm^{-1} was selected as this is the strongest peak at elevated temperature ($\sim 1000\text{ K}$)

Selection guideline 4:

Further to maximizing the online absorption cross section, the offline cross section should be minimized to ensure the differential cross section, $\Delta\sigma$, is enhanced

Selection guideline 5:

The spacing between the two spectral locations, online and offline, should be minimized to ensure that the differential cross section of the interferences is constrained to zero

Selection guideline 6:

When a spectrally structured interferent (e.g. ethylene) is present, the absorption cross-sectional spectrum requires careful inspection to seek exactly where the offline location should be chosen to result in zero differential cross section of the structured interferent at the temperature of concern. This principle should be used in conjunction with guideline 5 to seek the best combination of online and offline wavelengths

3 Experimental method

The experimental arrangement is shown in Fig. 4. The radiation source is an external cavity quantum-cascade laser (ECQCL) system (Daylight Solutions 11100-UT). The ECQCL was selected due to its wide tunability across target propene transitions over the spectral region of interest ($850\text{--}1000\text{ cm}^{-1}$), thus allowing for the best spectral locations (online and offline) to be used. The desired wavelength was achieved by regulating the injection current, laser head temperature, and diffraction grating orientation; such settings were governed via the ECQCL controller. The

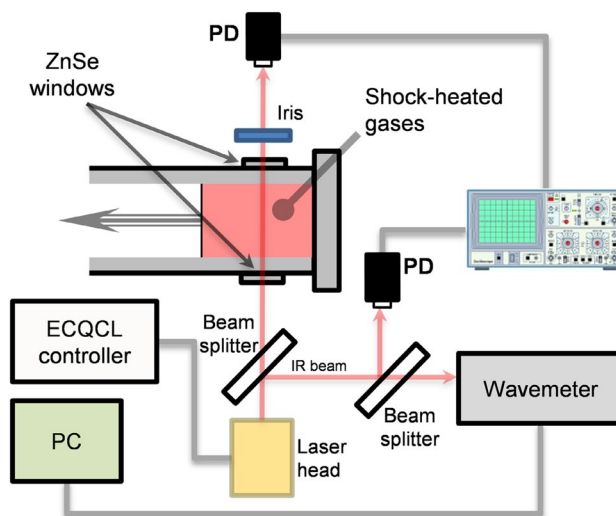


Fig. 4 Schematic of laser absorption measurements for in situ detection of propene. ECQCL external cavity quantum-cascade laser, PC personal computer, PD photo-detector

ECQCL used here was restricted to pulsed operation and was set with a $10\text{-}\mu\text{s}$ period (corresponding to the laser's maximum pulse repetition rate of 100 kHz) and a 0.6% duty cycle. The pulsed laser beam emerging from the head was split using a ZnSe plate, with the secondary reflected beam directed towards a calibrated wavemeter (Bristol 721) used to monitor the absolute wavelength during the course of an experiment. The tertiary beam emerging from a second ZnSe plate was directed to a thermoelectrically cooled photovoltaic detector (Vigo PVM 2TE-10.6/MPDC-F-10), in order to monitor laser intensity pulse-to-pulse fluctuation for the purpose of common-mode rejection.

The primary beam from the first ZnSe plate was directed through a shock tube via two ZnSe windows towards another similar photodetector. The path traversed through the shock tube corresponds to an inner diameter of 14.2 cm . These experiments were performed in the stainless steel, low-pressure shock tube facility at King Abdullah University of Science and Technology (KAUST). The shock tube is made of a 9-m driver section and a 9-m modular driven section. The incident shock speed is measured using a series of five piezoelectric PCB pressure transducers over the final 1.3 m of the shock tube. Reflected shock temperatures (T_5) and pressures (P_5) are determined from the measured incident shock speed and the standard 1D shock-jump relations. Further details of this shock tube can be found elsewhere [4, 13].

The procedure for determining the propene concentration, X_{propene} , inside the shock tube is as follows. Firstly, the shock tube was evacuated using a turbomolecular vacuum pump. The ECQCL is switched on with the appropriate wavelength selected near $10.9\text{ }\mu\text{m}$ (close to the transitions

used in our experiment). The driven section of the shock tube is then filled with a gaseous mixture of *n*-butane/argon up to a low pressure of ~ 50 Torr, depending on the desired post-reflected shock conditions. Finally, the driver section of the shock tube is pressurized with helium gas until the polycarbonate diaphragm, separating the driver and driven sections, ruptures. A shock wave consequently propagates through the driven section containing the low-pressure *n*-butane/argon mixture. This incident shock is reflected back from the end wall of the driven section. Absorption measurements are performed in the gases, behind the reflected shock wave, at a location 2 cm offset from the end wall. The transmitted irradiance through the shock tube is recorded on an oscilloscope (Tektronix DPO4104B, 5 GS/s, 1 GHz), and this is used as the signal, I , as per the Beer–Lambert relation $\alpha = \ln(I_0/I)$, where I_0 corresponds to absorption-free transmission and α is the absorbance arising from propene and interferents. The signal I_0 is taken from the secondary photodetector used for common-mode rejection, and hence, both I and I_0 can be recorded synchronously during a single shock. Absorbance, α , is measured twice for both online and offline spectral wavelengths of 912.18 and 918.3 cm^{-1} , respectively. This required two separate shocks to be repeated for the online and offline spectral measurements, which require the two repeated experiments to be at similar post-shock conditions of T_5 and P_5 . The absorbances, α_{online} and α_{offline} , can then be used to infer the differential absorbance, $\Delta\alpha$, from Eq. 3. Having knowledge of absorption cross sections, σ and $\Delta\sigma$, and thermodynamic conditions of the experiments (i.e. T_5 and P_5), the propene concentration, X_{propene} , can then be inferred from Eq. 4.

4 Results and discussion

4.1 Cross-sectional measurements and interference characterization

Precise knowledge of absorption cross sections is a necessary step to determining propene composition, as per Eq. (4). Experimentally, determined cross section, $\sigma(T)$, is required because detailed theoretical spectroscopic data from HITRAN are unavailable for relatively large molecules, such as propene (C_3H_6). Figure 5a shows measured absorption cross sections for online and offline spectral locations as a function of temperature and pressure.

For both online and offline, the profile of $\sigma(T)$ decreases monotonically in the temperature range 800–2000 K. This trend is reproduced at different pressures in the range 0.8–7.2 bar, thus rendering $\sigma(T)$ to be pressure independent in this range of interest. This is to be expected due to the large number of overlapping absorption lines within the spectrum, which renders the spectrum more immune to

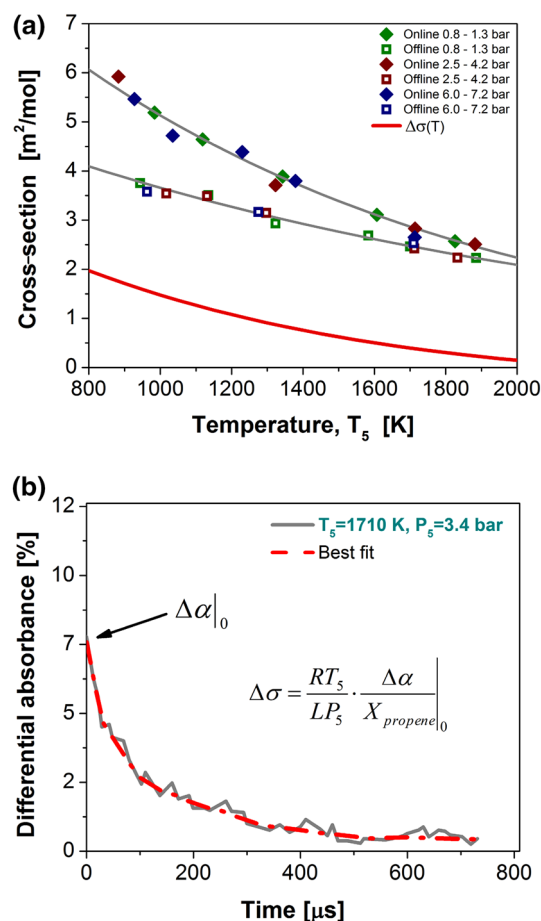


Fig. 5 **a** Measured absorption cross sections of propene at online (912.18 cm^{-1}) and offline (918.3 cm^{-1}) wavelengths for pressures ranging 0.8–7.2 bar and temperatures ranging 900–1900 K. The red trace is the inferred differential (online–offline) cross section, $\Delta\sigma$. Measurements are taken using a 5 % propene/argon mixture behind reflected shock waves. **b** Example time trace of propene pyrolysis, showing how $\Delta\sigma$ relates to the initial value of differential absorbance

changes in pressure, unlike isolated spectral lines. The differential cross section, $\Delta\sigma(T)$, shown in Fig. 5a is calculated from the difference of the online and offline cross sections. Figure 5b shows an example time trace of differential absorbance corresponding to the case with initial conditions of $T_5 = 1710$ K, $P_5 = 3.4$ bar, 5 % propene in argon. It is illustrated in Fig. 5b that the cross section $\Delta\sigma(T)$ is based on initial conditions as indicated at time zero, since the propene concentration is known at this moment before pyrolysis progresses. It should be noted that at elevated temperatures, the online cross section, which was chosen based on one of the peak values at room temperature shown in Fig. 3b, becomes smaller and thus results in modest values of the differential cross section. The clearly identifiable trends of the cross sections were fitted for both wavelengths; this enabled an empirical relationship to be derived for the differential cross section:

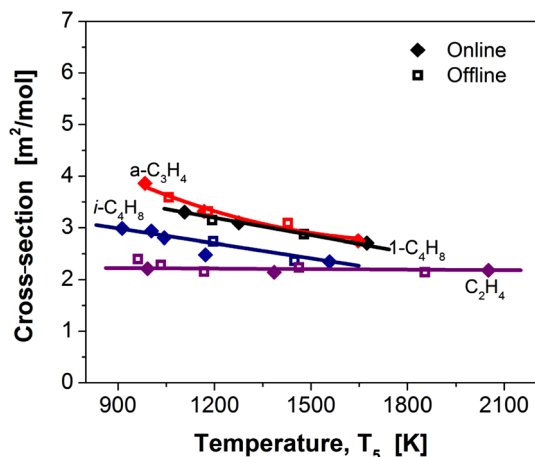


Fig. 6 Measured absorption cross sections of potential interfering species: C_2H_4 (ethene), $1-C_4H_8$ (1-butene), $i-C_4H_8$ (*iso*-butene), $a-C_3H_4$ (allene) for online (912.18 cm^{-1}) and offline (918.3 cm^{-1}) wavelengths, showing almost identical values across a range of temperatures. These measurements are taken using 5 %/argon mixtures behind reflected shock waves

$$\Delta\sigma(T) = \Delta\sigma_o \left(\frac{T_o}{T}\right)^{2.02} \quad \Delta\sigma_o = 1.35\text{ m}^2\text{mol}^{-1}; \quad T_o = 1000\text{ K} \quad (5)$$

For the technique to work properly, it is important to verify that the differential cross sections of the likely interferents encountered in the pyrolysis of a fuel (e.g. *n*-butane in this study) are negligible. Figure 6 shows measured absorption cross sections of species typically present during pyrolysis of *n*-butane. The presence of such potential interfering molecules was postulated using chemical kinetic simulations invoking the JetSurF 1.0 mechanism [27].

These large molecules indeed exhibit zero differential absorption cross section, as manifested in Fig. 6 by the overlapping traces for online and offline cases. This is expected owing to larger molecules possessing spectra with a greater density of absorption lines, hence, promoting relatively broad and featureless aggregate spectra at pressures exceeding a few hundred Torr. Such aggregate spectra are exemplified in Fig. 3b for 1-butene and 2-butene. However, more importantly, the differential cross section for the smaller interfering molecule of ethylene (C_2H_4) can also be set to zero through judicious choice of online and offline spectral locations. The case of ethylene requires care due to the more uneven spectral structure, and thus, it is important to deliberately select the right combination of locations that will result in equal online and offline absorption cross sections. This was achieved in our study and manifested by the purple trace in Fig. 6. It is also observed that ethylene cross sections are weakly dependent on temperature at these two wavelengths.

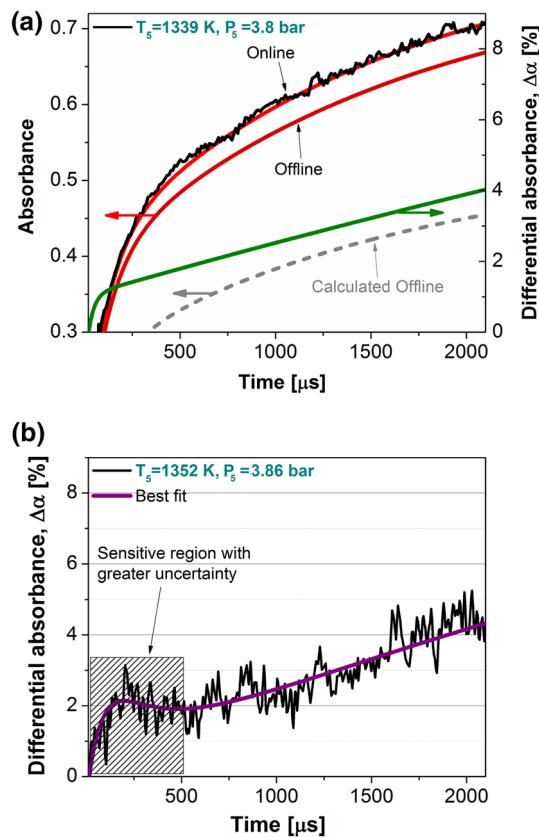


Fig. 7 **a** Measured online and offline propene absorbances for pyrolysis of 5 % *n*-butane in argon at $T_5 = 1339\text{ K}$, $P_5 = 3.8\text{ bar}$. The differential absorbance (green) is portrayed by the difference between the two lines of best fit (red). The dashed grey line represents the offline absorbance based on calculations using the JetSurF 1.0 mechanism [27]. **b** Another example of a differential absorbance trace at similar conditions ($T_5 = 1352\text{ K}$, $P_5 = 3.86\text{ bar}$), where non-monotonic behaviour is exhibited in the first 500 μs

4.2 Diagnostic demonstration

After the characterization of differential cross sections, experiments of *n*-butane pyrolysis were performed behind reflected shock waves. Figure 7a shows traces of absorbance (α_{online} , α_{offline} and $\Delta\alpha$), for example pyrolysis case of 5 % *n*-butane/argon mixture at post-shock conditions of $T_5 = 1339\text{ K}$ and $P_5 = 3.8\text{ bar}$. The black trace corresponds to experimental data, shown alongside a corresponding exponential curve fit (red trace). Only one experimental noisy data trace is shown in Fig. 7a for the purpose of maintaining graphical clarity. From the red traces, one observes a general increasing trend of absorbance with time. It should be noted that this absorbance is the composite of the propene and underlying contributions from all interfering molecules. The small detectable difference between the online and offline traces equates to the differential absorbance, $\Delta\alpha$, depicted as the green trace in Fig. 7a. The green trace essentially represents interference-free propene

absorbance varying with time over a 2-ms interval, rising up to $\Delta\alpha \approx 4\%$.

The low magnitude of the differential absorbance, $\Delta\alpha$, shown in Fig. 7a is due to the small difference between the measured offline and online traces. This small difference arises due to the relatively large offline absorption contribution. A qualitative calculation of the offline absorbance, based on modelled species mole fractions, can shed light on the nature of the offline profile. Such a calculation uses indicative values of cross sections for the interferents from Fig. 6 and for offline propene from Fig. 5a; modelled mole fractions of the species were taken from the JetSurF 1.0 mechanism [27]. The dashed grey trace in Fig. 7 (a) depicts the *calculated* offline profile, whereby there is an evident departure from the measured offline profile (red trace) of $\sim 33\%$ at $t = 2$ ms. The difference is attributable to either (1) the omission of some interferents in the calculation, or (2) the overall under-prediction of mole fractions from the model. Such a disparity between measured and modelled results demonstrates the continued need for quantitative experimental data to improve the fidelity of reaction mechanisms.

4.2.1 Early time behaviour

Figure 7b shows the evolution of $\Delta\alpha$ over the same time interval of 2 ms, with the black and purple traces representing the experimental trace and curve fit, respectively. This plot of differential absorbance corresponds to conditions (i.e. $T_5 = 1352$ K, $P_5 = 3.86$ bar) very similar to that of Fig. 7a. Evidently, the overall trend of the two traces of $\Delta\alpha$ in Fig. 7a and b is very similar, except for the first 500 μs . It is expected that the two traces would be identical qualitatively, yet, in the region $t < 500$ μs , there is a clear deviation from monotonic behaviour with an initial rise then a dip before the overall trend of increasing $\Delta\alpha$ is recovered. This discrepancy between traces of $\Delta\alpha$ for similar post-shock conditions suggests that the initial non-monotonic trend is likely to be an artefact, corroborated by monotonic trends seen in time histories of propene derived from the JetSurF 1.0 mechanism [27] at similar conditions. Because of such a disturbance in the profile at early times, it could be entertained that the effect is attributable to vibrational non-equilibrium arising from the passing shock wave. However, for large molecules such as propene, equilibration times are 10–50 ns, which are typical for hydrocarbons [30, 31]. Such timescales are four orders of magnitude shorter than the initial 500 μs period, and therefore render vibrational non-equilibrium to not be a problem.

For the measurement of propene absorption cross sections in Sect. 4.1, an accompanying example time profile of how propene pyrolysis typically progresses was shown

in Fig. 5b. On comparison of Fig. 7b with Fig. 5b, it is apparent that pyrolysis of propene does not exhibit non-monotonic time behaviour unlike pyrolysis of *n*-butane, when our differential absorption laser diagnostic is applied. To account for the difference, one may postulate that the early time behaviour seen during *n*-butane pyrolysis may be attributable to unaccounted spectral interference from an intermediate. However, upon more careful consideration, this is unlikely given that we do not observe any obvious interference in the case of propene pyrolysis. When a hydrocarbon with an extra carbon atom, such as *n*-butane, undergoes pyrolysis, the next class of potential interferents is one containing four carbon atoms (e.g. *i*-C₄H₈, 1-C₄H₈, 2-C₄H₈). Because this class of interferents is based on larger molecules, their spectral structure is quite broad, rendering it easier to guarantee equivalent cross sections for both online and offline spectral locations that are reasonably close together, as exhibited in Fig. 6. Therefore, the likelihood of the undulation seen in Fig. 7b due to an unaccounted intermediate is quite improbable.

We contemplate a more plausible reason as to why such undulation occurs in our profiles of differential absorbance at early times. Through inductive reasoning, we posit three necessary and sufficient conditions to be satisfied that leads to the early time behaviour to occur, namely (1) the existence of a narrowing gap between the online and offline absorbance profiles (α_{online} and α_{offline}) leading to a pinch point towards time zero (see red traces in Fig. 7a), (2) steep gradients of these curves in the vicinity of the pinch point, and (3) randomized undulations in the traces of α_{online} and α_{offline} caused by beam steering. In Fig. 7a, we can clearly see the gradients of the red curves are both steep and that they are in close proximity, and so, any undulation is amplified in this region of early times when the two curves are subtracted from one another. Alternatively, for the case of propene pyrolysis shown in Fig. 5b, we do not readily observe amplified undulation at early times in the differential result. This is because at early times, all three criteria are not simultaneously satisfied in the case of propene pyrolysis. At early times, there are steeper gradients and undulations will exist. However, the pinch point now occurs as $t \rightarrow \infty$, where the gradients diminish towards zero. Because a finite nonzero differential absorbance exists between the two constituent absorbance curves for early times, in spite of the presence of steep gradients in this region, there is less potential for undulation to be amplified in the case of propene pyrolysis.

Nevertheless, a possible method to mitigate the influence of beam steering-induced undulation is to measure online and offline absorbance profiles simultaneously during the passing of a single shock wave. This could be achieved by overlapping two laser beams, corresponding to the online

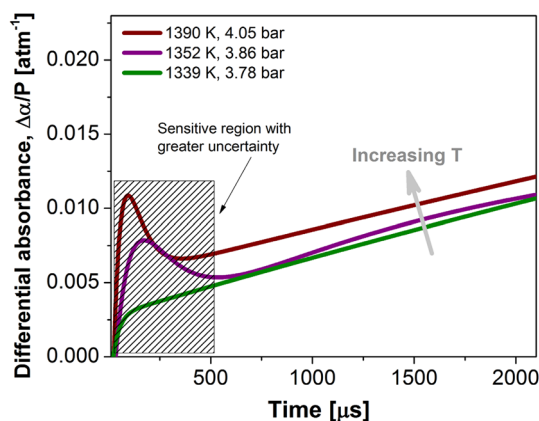


Fig. 8 Lines of best fit for three measurements of pressure-normalized differential absorbance at similar temperatures showing greatest variance, and hence uncertainty, near time zero. These measurements are taken using 5 % *n*-butane in argon behind reflected shock waves

and offline wavelengths and directing the overlapping pair through the shock tube. This would result in both beams to experience the same degree of beam steering during one experiment and would therefore result in the cancellation of the effect of beam steering-induced undulation in the differential absorbance profiles. This strategy could not be achieved in the current work owing to the availability of only a single laser.

Figure 8 displays three time profiles, relating to differential absorbance, for *n*-butane pyrolysis at similar temperatures and pressures. Such curves manifest the variability, and hence confirm the unreliability, of the sensitive region at early times (shaded in Fig. 8). Because $\Delta\alpha$ scales directly with pressure, the traces are normalized with respect to P_5 , to facilitate comparison of trends with temperature, T_5 . Clearly, there is a region within the first ~ 500 μs where there is a higher degree of variance in the monotonicity of the trends, as initially demonstrated in Fig. 7b. Figure 8 exhibits traces of $\Delta\alpha/P$ derived from curves of best fit, instead of showing experimental data traces which would otherwise obscure the small differences between the traces at slightly different temperatures.

Looking at Fig. 8, one can postulate that the appearance of the shoulder at early times is temperature dependent and it is a genuine kinetic effect. However, we consider this to be implausible. Firstly, there is a ~ 100 % difference between the green and violet curves at $t = 150$ μs , which could not have been caused by a mere 13 K (or 0.97 %) change in temperature, from 1339 to 1352 K. Secondly, evidence from multiple sources [11, 23, 25, 32–34] describing the pyrolysis of various stable hydrocarbon molecules predisposes the existence of monotonic-only behaviour with time, in contrast to what is otherwise seen in the two traces of Fig. 8.

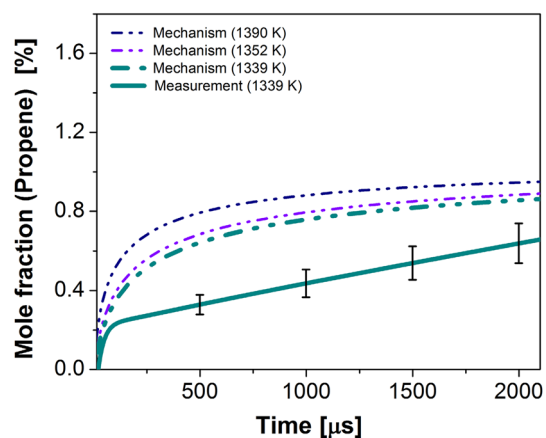


Fig. 9 Comparison of our measured propene mole fraction as a function of time against that calculated from the JetSurF 1.0 mechanism for T_5 : 1339–1390 K around pressures of 3.5 bar

4.2.2 Overall profile behaviour

Nevertheless, outside of the shaded region shown in Fig. 8, there appears to be an overall trend in which $\Delta\alpha/P$ increases with temperature, T_5 , as denoted by the arrow of increasing T . Because propene mole fraction, X_{propene} , is proportional to $\Delta\alpha$, and the temperature is essentially constant in time [i.e. $T(t) = T_5$] for idealized conditions and dilute gaseous mixtures in the shock tube, it is expected that there is a qualitative agreement between traces of $\Delta\alpha/P$ in Fig. 8 and that of X_{propene} with time. The measured absorbance of propene is converted to mole fraction using Eq. (4) and compared with kinetic simulations in Fig. 9.

The simulated evolution of propene mole fraction, employing the JetSurF 1.0 mechanism [27], for the three temperatures investigated in this study is shown by the dashed lines in Fig. 9. For a given point in time, the traces exhibit a clear increase in X_{propene} with temperature over the interval 1339–1390 K. This is in qualitative agreement with the trends of $\Delta\alpha/P$ in Fig. 8. Furthermore in Fig. 9, we show one of the traces of experimentally determined propene mole fraction corresponding to the case of $T_5 = 1339$ K. The error bars superimposed onto the experimental trace show the range of values that the trace could adopt within one standard deviation of X_{propene} . It is also noteworthy that the experimentally derived mole fraction appears to be systematically lower than that simulated by the mechanism, exemplified by a 100 % deviation at $t = 1$ ms.

Further support for the credibility of the overall trend of the derived propene time trace, seen in Fig. 9, can be sought by examining the nature of the offline absorbance profile. Similar to Fig. 7a, Fig. 10 displays the measured offline

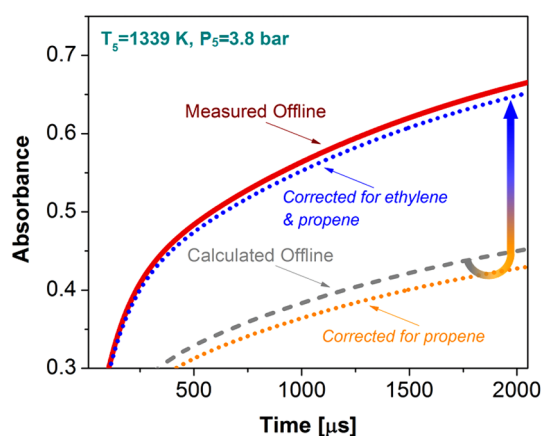


Fig. 10 Measured offline absorbance (red trace) for pyrolysis of 5 % *n*-butane in argon at $T_5 = 1339$ K, $P_5 = 3.8$ bar. Dashed grey trace represents the calculated offline absorbance based on the JetSurF 1.0 mechanism. Dotted orange and blue traces represent corrections to the grey calculated offline profile based on our measured propene trace in Fig. 9 and upper estimates of ethylene from the literature [23, 25]

profile (red trace), as well as the calculated offline profile (grey trace) based on data from the JetSurF 1.0 mechanism [27], for 5 % *n*-butane pyrolysis at $T_5 = 1339$ K and $P_5 = 3.8$ bar. Our results exhibit self-consistency, as demonstrated in the following argument.

By considering the two major species contributors (i.e. C_3H_6 and C_2H_4) to absorbance at the offline wavelength, the apparent discrepancy between the measured and calculated offline profiles in Fig. 10 can be resolved. Chemical kinetic mechanisms, such as JetSurF, do not always yield accurate predictions of species profiles. Given that the calculated offline profile is based on mole fraction data from JetSurF 1.0 [27], it would be instructive to examine the effect of correcting the propene and ethylene mole fractions derived from the mechanism. Firstly, the predicted propene mole fraction is substituted with our measured result from Fig. 9; the result of the correction to the calculated offline profile is portrayed as the dotted orange trace in Fig. 10, with an accompanying 3 % drop in absorbance from the grey trace at $t = 2$ ms. Secondly, the predicted ethylene mole fraction is doubled; this is judged as a conservative upper estimate based on circumstantial evidence in the literature. The JetSurF mechanism seemingly underestimates intermediates, including ethylene, by as much as 100 % for fuel pyrolysis [23, 25]. The end result is shown as the dotted blue trace in Fig. 10, where the curled arrow depicts the transition from the original calculated offline profile (grey trace) via the two corrections for propene and ethylene. After such an adjustment for mole fractions, the departure of the calculated offline profile (dotted blue trace) from the measured profile (red trace) is significantly smaller. The largest contribution

to (online and offline) absorbance is ethylene, and it subsequently seems that the magnitude of the offline profile is plausible, lending credence to the relatively small differential absorbance values observed earlier in Figs. 7 and 8 and the associated propene time profile in Fig. 9.

Apart from the abovementioned argument of self-consistency, Fig. 10 also draws attention to the relatively large contribution of ethylene to the absorbance profile. It transpires that if the adjustment for mole fraction in Fig. 10 reflects reality, the relative contribution of ethylene is ~75 % of the total offline absorbance. It is curious to note that if the background contribution from ethylene could hypothetically be suppressed during a measurement, the total absorbance would be reduced by a factor of four. Considering the nonlinear nature of the Beer–Lambert law, it can be argued that for the same degree of differential absorbance and lower total absorbance, the SNR of the resulting propene mole fraction trace would then be improved. This is particularly relevant to the case of larger hydrocarbon pyrolysis which would result in absorbance signals being swamped by contributions from large amounts of ethylene, amongst other interferences.

5 Summary and future work

A diagnostic strategy, based on differential absorption, was developed to quantify mole fraction of propene (C_3H_6) in combustion gases. It is an initial endeavour to employ a laser absorption diagnostic to measure the rapid evolution of such a hydrocarbon species within a shock tube environment. This was achieved through an initial measurement of absorption cross sections at online and offline spectral positions. Through judicious choice of the spectral positions, interference-free measurements of the propene mole fraction can be achieved. Propene mole fraction time profiles were also compared to that simulated by a well-studied chemical kinetic mechanism, and such an experimental diagnostic is a first step in helping to further spur the development and refinement of such kinetic models. It is suggested that further work could entail optimizing the differential cross section used in the diagnostic by selecting alternative spectral line positions. In a similar vein to improve SNR, a method to suppress background absorbance from interferences could be investigated. However, most importantly, our initial endeavour to employ the differential absorption technique could be further developed to overcome the undesired early time behaviour observed in the propene measurements. It is, therefore, recommended that online and offline optical measurements be conducted synchronously during the passing of a reflected shock wave to evade the effects of beam steering.

Acknowledgments The authors would like to acknowledge King Abdullah University of Science and Technology (KAUST) and Saudi Basic Industries Corporation (SABIC) for research funds towards this project.

References

1. A.P. Dowling, *Aeronaut. J.* **104**, 105 (2000)
2. R.S.M. Chrystie, I.S. Burns, C.F. Kaminski, *Combust. Sci. Technol.* **185**, 180 (2013)
3. R.K. Hanson, D.F. Davidson, *Prog. Energy Combust. Sci.* **44**, 103 (2014)
4. R.S.M. Chrystie, E.F. Nasir, A. Farooq, *Proc. Combust. Inst.* **35**, 3757 (2015)
5. M.B. Sajid, E.T. Es-sebbar, T. Javed, C. Fittschen, A. Farooq, *Int. J. Chem. Kin.* **46**, 275 (2014)
6. R.S.M. Chrystie, E.F. Nasir, A. Farooq, *Opt. Lett.* **39**, 6620 (2014)
7. H. Wang, D.A. Sheen, *Combust. Flame* **158**, 645 (2011)
8. D. Bradley, M. Lawes, M.S. Mansour, *Proc. Combust. Inst.* **33**, 1269 (2011)
9. IPCC Special Report: Safeguarding the Ozone Layer and the Global Climate System (Cambridge University Press 2014)
10. S.S. Vasu, Z. Hong, D.F. Davidson, R.K. Hanson, D.M. Golden, *J. Phys. Chem. A* **114**, 11529 (2010)
11. R.M. Spearrin, S. Li, D.F. Davidson, J.B. Jeffries, R.K. Hanson, *Proc. Combust. Inst.* **35**, 3645 (2015)
12. S.M. Burke, W. Metcalfe, O. Herbinet, F. Battin-Leclerc, F.M. Haas, J. Santner, F.L. Dryer, H.J. Curran, *Combust. Flame* **161**, 2765 (2014)
13. J. Badra, A.E. Elwardany, F. Khaled, S. Vasu, A. Farooq, *Combust. Flame* **161**, 725 (2014)
14. C.-W. Zhou, Z.-R. Li, X.-Y. Li, *J. Phys. Chem. A* **113**, 2372 (2009)
15. J. Zador, A.W. Jasper, J.A. Miller, *Phys. Chem. Chem. Phys.* **11**, 11040 (2009)
16. L.K. Huynh, H.R. Zhang, S. Zhang, E. Eddings, A. Sarofim, M.E. Law, P.R. Westmoreland, T.N. Truong, *J. Phys. Chem. A* **113**, 3177 (2009)
17. C. Kappler, J. Zádor, O. Welz, X. Fernandez Ravi, M. Olzmann, A. Taatjes, Z. Craig, *Phys. Chem.* **225**, 1271 (2011)
18. W.B. Kindzierski, C.C. Small, F. Yi, M.A. Bari, Z. Hashisho, *Automotive wastes. Water Environ. Res.* **84**, 1407 (2012)
19. C.K. Westbrook, W.J. Pitz, H.J. Curran, *J. Phys. Chem. A* **110**, 6912 (2006)
20. C. Ji, S.M. Sarathy, P.S. Veloo, C.K. Westbrook, F.N. Egolfopoulos, *Combust. Flame* **159**, 1426 (2012)
21. X. He, S.M. Walton, B.T. Zigler, M.S. Wooldridge, A. Atreya, *Int. J. Chem. Kin.* **39**, 498 (2007)
22. A. Samman, S. Gebremariam, L. Rimai, X. Zhang, J. Hangas, G.W. Aunner, *Sens. Actuators, B* **63**, 91 (2000)
23. S.H. Pyun, J. Cho, D.F. Davidson, R.K. Hanson, *Meas. Sci. Technol.* **22**, 025303 (2011)
24. M.B. Sajid, T. Javed, A. Farooq, *J. Quant. Spectrosc. Radiat. Transfer* **155**, 66 (2015)
25. M.E. MacDonald, W. Ren, Y. Zhu, D.F. Davidson, R.K. Hanson, *Fuel* **103**, 1060 (2013)
26. I. Stranic, R.K. Hanson, *J. Quant. Spectrosc. Radiat. Transfer* **142**, 58 (2014)
27. B. Sirjean et al. *JetSurF 1.0*, (<http://web.stanford.edu/group/haiwanglab/JetSurF/JetSurF1.0/index.html>) (2009)
28. CHEMKIN-PRO 15112, Reaction Design: San Diego, (2011)
29. E.T. Es-sebbar, M. Alrefae, A. Farooq, *J. Quant. Spectrosc. Radiat. Transfer* **133**, 559 (2014)
30. C.F. Wang, G.S. Springer, *J. Chem. Phys.* **59**, 6556 (1973)
31. J.H. Kiefer, G.C. Sahukar, S. Santhanam, N.K. Srinivasan, R.S. Tranter, *J. Chem. Phys.* **120**, 918 (2004)
32. K. Yasunaga, Y. Kuraguchi, R. Ikeuchi, H. Masaoka, O. Takahashi, T. Koike, Y. Hidaka, *Proc. Combust. Inst.* **32**, 453 (2009)
33. Y. Zhang, J. Cai, L. Zhao, J. Yang, H. Jin, Z. Cheng, Y. Li, L. Zhang, F. Qi, *Combust. Flame* **159**, 905 (2012)
34. W. Ren, D. Davidson, R. Hanson, *Int. J. Chem. Kin.* **44**, 423 (2012)